Computer Assisted Mechanics and Engineering Sciences, 6: 263–277, 1999.


# Numerical solution for laminar unsteady flow about fixed and oscillating cylinders

László Baranyi
*Department of Fluid and Heat Engineering, University of Miskolc, H-3515 Miskolc-Egyetemváros, Hungary*

Masataka Shirakashi
*Department of Mechanical Engineering, Nagaoka University of Technology, 1603-1 Kamitomioka, Nagaoka, 940-2188 Japan*

(Received March 8, 1999)

This paper presents a finite-difference solution of the two-dimensional, time dependent incompressible Navier–Stokes equations for laminar flow about fixed and oscillating cylinders placed in an otherwise uniform flow. Using boundary fitted coordinates, the equations are transformed to a non-inertial reference frame fixed to the cylinder. The primitive variable formulation is used for the solution of the problem. A special transformation provides a fine grid scale near the cylinder walls and a coarse grid in the far field. Forward difference is used in time, fourth order central difference in space except for convective terms for which a modified third-order upwind scheme is used. Velocity values are obtained explicitly, and the successive over-relaxation (SOR) method yields the pressure distribution. Computed drag coefficients and dimensionless vortex shedding values were compared with experimental results for rigid cylinders and a very good agreement has been obtained. Amplitude bounds of locked-in vortex shedding due to forced crossflow oscillation of a circular cylinder are also determined for $Re = 180$.

**Keywords:** incompressible flow, Navier–Stokes equations, unsteady flow, laminar flow, bluff body, lock-in

## 1. Introduction

Flow about bluff bodies has received much experimental, analytical and numerical study due to its practical importance. When a bluff body is exposed to the flow, vortices are shed from both sides of the body into the wake. This vortex shedding gives rise to a periodic lift force acting on the body. When the frequency of vortex shedding coincides with the natural frequency of the body, large amplitude oscillation or resonance can occur. This phenomenon is known as Kármán vortex excitation, synchronization or lock-in. This type of oscillation can be observed in many engineering practices, e.g. structures placed in the flow of air or liquid, or flow around the tubes of heat exchangers and other equipment. That is the reason why much effort has been devoted to clarify the mechanism of vortex excitation. This is of primary importance if one wishes to predict this phenomenon and to develop methods for suppressing or controlling the exciting forces. Numerical studies of vortex shedding first have primarily addressed the flow of a uniform stream normal to a rigid circular cylinder [9, 2, 8]. Since the cylinder is fixed, no information about vibration interaction is thus obtained. If the cylinder is vibrating, either in forced or in natural motion, a nonlinear interaction occurs as the cylinder frequency approaches the vortex shedding frequency. The major characteristic of this interaction is that the natural shedding frequency is suppressed and vortex shedding occurs instead at the cylinder vibration frequency over a range of flow velocities. This is known as lock-in or synchronization phenomenon. This effect occurs when the cylinder is vibrating either transverse or in-line with the freestream direction. The

lock-in range is somewhat dependent on Reynolds number and oscillation amplitude of cylinder. There are several methods worked out for the investigation of lock-in phenomenon and near wake flows [7, 3, 12, 11]. Some of the more recent advances on the investigations of bluff body flows are reviewed in [1].

The present study transforms the Navier–Stokes equations to a non-inertial reference frame fixed to the oscillating cylinder placed in an otherwise uniform stream, thus simplifying the boundary condition specification. The transformed equations are solved by finite difference method. Results for flow about fixed cylinder is compared with those of experiments. Amplitude bounds of locked-in vortex shedding due to forced crossflow oscillation of a circular cylinder are also determined for $Re = 180$.

### 1.1. Nomenclature

$a_0$ – acceleration of cylinder oscillation
$C_D$ – drag coefficient $(= C_{Dp} + C_{Df})$
$C_{Df}$ – skin friction drag coefficient
$C_{Dp}$ – pressure drag coefficient
$C_L$ – lift coefficient $(= C_{Lp} + C_{Lf})$
$C_{Lf}$ – skin friction lift coefficient
$C_{Lp}$ – pressure lift coefficient
$D$ – cylinder diameter (length scale $L$)
$f_c$ – frequency of cylinder oscillation, nondimensionalized by $U/D$
$f_v$ – frequency of vortex shedding, nondimensionalized by $U/D$
$J$ – Jacobian
$L$ – length scale $(= D)$
$p$ – pressure, nondimensionalized by $\rho U^2$
$R$ – radius, nondimensionalized by $D$
$Re$ – Reynolds number, $UD/\upsilon$
$S$ – Strouhal number, $f_v D/U$
$t, \tau$ – time, nondimensionalized by $D/U$
$\Delta t$ – time step
$u, v$ – velocities in $x$ and $y$ directions, nondimensionalized by $U$
$x, y$ – Cartesian coordinates, nondimensionalized by $D$
$\alpha, \gamma, \varphi, \sigma$ – metric parameters
$\xi, \eta$ – general curvilinear coordinates
$\Theta$ – dilation
$\varphi$ – angle around the cylinder from the point facing downstream

### 1.2. Subscripts

$i, j$ – denotes position
$n$ – components in the direction of the outer normal
pot – refers to potential flow
$x, y$ – denotes vector components or differentation in $x$ and $y$ directions, respectively
$\xi, \eta$ – denotes vector components or differentation in $\xi$ and $\eta$ directions, respectively
0 – refers to the motion of the cylinder
$\infty$ – denotes conditions at infinity

## 2. Governing equations

The primitive variable formulation is used for the solution of the problem. The governing equations are: two components of the non-conservation form of the Navier–Stokes equations and the equation of continuity. These equations contain only dimensionless quantities and they can be written as follows [13]

$$\frac{\partial u}{\partial t} + u\frac{\partial u}{\partial x} + v\frac{\partial u}{\partial y} = -\frac{\partial p}{\partial x} + \frac{1}{Re}\left(\frac{\partial^2 u}{\partial x^2} + \frac{\partial^2 u}{\partial y^2}\right) - a_{0x}\,; \tag{1}$$

$$\frac{\partial v}{\partial t} + u\frac{\partial v}{\partial x} + v\frac{\partial v}{\partial y} = -\frac{\partial p}{\partial y} + \frac{1}{Re}\left(\frac{\partial^2 v}{\partial x^2} + \frac{\partial^2 v}{\partial y^2}\right) - a_{0y}\,; \tag{2}$$

$$\Theta = \frac{\partial u}{\partial x} + \frac{\partial v}{\partial y} \qquad = 0. \tag{3}$$

The Navier–Stokes equations are written for a two-dimensional laminar flow in the non-inertial coordinate system fixed to the cylinder oscillating with acceleration $a_0$. In this way we can avoid the necessity of interpolating the initial conditions for the grid points at every time step. Although equations are derived for an oscillating cylinder, naturally all of our forthcoming derivations remain valid for flow about fixed cylinder as well. In this case we simply substitute $a_0 = 0$ into our equations.

The major difficulty in obtaining a time-accurate solution for an incompressible flow arises from the fact that the continuity equation does not contain the time derivative explicitly [10]. This difficulty can be overcome by introducing a separate equation for pressure. By adding the $x$-derivative of Eq. (1) and $y$-derivative of Eq. (2), rearranging it, and neglecting all terms related to $\Theta$ except its partial derivative with respect to time $t$, finally yields a Poisson equation for pressure [13]

$$\frac{\partial^2 p}{\partial x^2} + \frac{\partial^2 p}{\partial y^2} = 2\left[\frac{\partial u}{\partial x}\frac{\partial v}{\partial y} - \frac{\partial u}{\partial y}\frac{\partial v}{\partial x}\right] - \frac{\partial \Theta}{\partial t}\,. \tag{4}$$

Although strictly the dilation $\Theta = 0$ by continuity (3), but in the primitive variable formulation when the finite difference scheme does not exactly conserves mass due to truncation errors then these terms may be non-zero. In this case it is advisable to retain some terms containing dilation to give a correction to dilation and avoid instability [5]. Our careful numerical investigation has revealed the fact that all terms containing $\Theta$ except $\partial\Theta/\partial t$ have negligible effect on the solution. This is the reason why only this term was retained in Eq. (4). Equations (1), (2) and (4) will be solved while the continuity Eq. (3) is satisfied at every time step.

The body force, which is assumed to be due to gravity only, does not appear in Eqs. (1) and (2) explicitly. This force is included in the pressure term $p$. In this way hydrodynamic and buoyancy forces acting on the body placed in the flow can be separated. The components of drag and lift due to pressure $p$ acting on the body mean the hydrodynamic components originated from the interaction of the body and viscous fluid-flow. The real lift acting on a body placed in a flow field can be obtained as the sum of the buoyancy force and the hydrodynamic lift obtained by the solution of Eqs. (1)–(4). As it can be proved easily the involvement of the body force into the pressure term does not influence the drag.

### 2.1. Boundary conditions

On the surface of the cylinder ($R_1$) (see Fig. 1):

- Velocity: no-slip condition

$$u = v = 0. \tag{5}$$

- Pressure:

$$\frac{\partial p}{\partial n} = \frac{1}{Re}\nabla^2 v_n - a_{on} \tag{6}$$

where $n$ refers to components in the direction of the outer normal. This expression is obtained from the Navier–Stokes equations of (1) and (2).

Far from the cylinder ($R_2$):

- Velocity: potential flow

$$\begin{aligned} u &= u_{\text{pot}} - u_0 \,, \\ v &= v_{\text{pot}} - v_0 \,, \end{aligned} \tag{7}$$

where $u_0$, $v_0$ means the velocity components of the oscillating cylinder, and subscript 'pot' stands for potential flow.

- Pressure:

$$\frac{\partial p}{\partial n} \cong \left(\frac{\partial p}{\partial n}\right)_{\text{pot}} . \tag{8}$$

It is to be noted that the assumption of potential flow in the far field region is reasonable except for the narrow wake. The outer boundary of the computational domain is very far from the cylinder, hence it is not surprising that our computational experience shows that these assumptions result in a small distortion of the velocity field near the outer boundary wake region only.

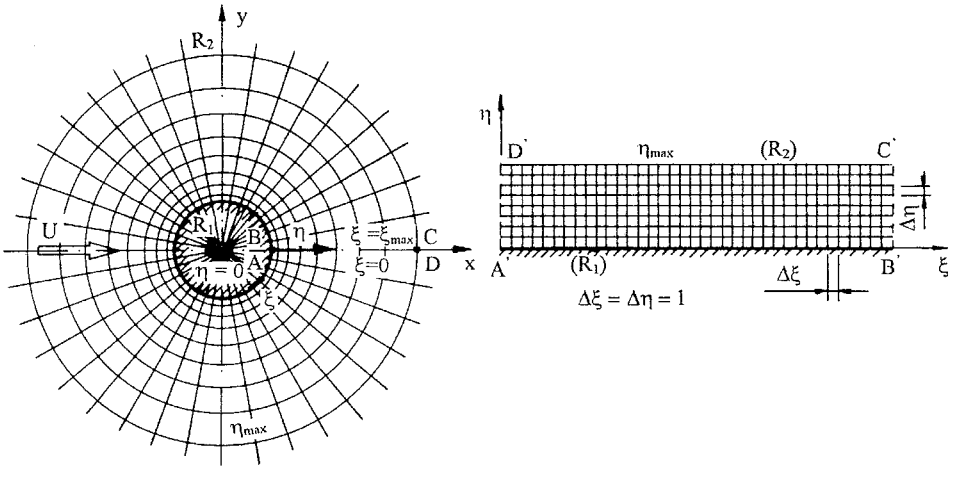


**Fig. 1.** Physical and computational planes

## 3. Transformation of the Governing Equations

Boundary conditions (BC) can be represented accurately when the boundary is such that it coincides with some coordinate line. In this case there is no need for interpolation. To avoid interpolation is particularly important for boundaries with strong curvature or slope discontinuity. The generation of a curvilinear coordinate system with coordinate lines coincident with all boundaries, called boundary fitted system, is thus an essential part of a general numerical solution of a partial differential equation (PDE) system. Any PDE system can be solved on the boundary fitted coordinate

system by transforming the set of PDEs and associated BCs to the curvilinear system. The transformed equations can be approximated for example by using finite difference expressions and solved numerically on the transformed plane.

First we have to transform the physical plane into the computational one. This will provide the computational meshes, too. Figure 1 shows these two planes.

We have chosen the way of description where both the coordinate system and the grid are fixed to the accelerating cylinder. This non-inertial system formulation has triple benefits:

- the computational grid has to be generated only once;
- since grid points are fixed even on the physical plane, there is no need for interpolation of the initial conditions at the beginning of every time step;
- the transformed governing equations have simpler forms.

A unique, single-valued relationship between the coordinates on the computational domain $(\xi, \eta, \tau)$ and the physical coordinates $(x, y, t)$ can be written as

$$\begin{aligned} x(\xi,\eta) &= R(\eta)\cos[g(\xi)], \\ y(\xi,\eta) &= -R(\eta)\sin[g(\xi)], \\ t &= \tau, \end{aligned} \tag{9}$$

where the dimensionless radius

$$R(\eta) = R_1 \exp[f(\eta)]. \tag{10}$$

This choice of the structure of the mapping function automatically assures that the obtained grid is orthogonal on the physical plane for arbitrary functions $f(\eta)$ and $g(\xi)$. At present our choice for functions $f(\eta)$ and $g(\xi)$ is as follows

$$g(\xi) = 2\pi\frac{\xi}{\xi_{\max}}, f(\eta) = \left[(1+a_1)\frac{\eta}{\eta_{\max}} - 2a_1\left(\frac{\eta}{\eta_{\max}}\right)^2 + a_1\left(\frac{\eta}{\eta_{\max}}\right)^3\right]\log\left(\frac{R_2}{R_1}\right), \tag{11}$$

where $a_1$ is a constant parameter, and subscript max stands for maximum value. If $a_1 = 0$ cylindrical coordinates with logarithmically spaced radial cells are obtained on the physical plane which provide a fine grid scale near the cylinder wall and a coarse grid in the far field. By changing the parameter $a_1$ we can control the grid resolution in the vicinity of the cylinder. The value of $a_1$ can not be arbitrary. Transformations (9), (10) are unique and single-valued only for non-vanishing Jacobian

$$J = y_\eta x_\xi - y_\xi x_\eta . \tag{12}$$

Taking into account this consideration parameter $a_1$ has to be chosen between the limits

$$-1 < a_1 < 3. \tag{13}$$

Finally, in the knowledge of the functional relationships (9)–(11), governing Eqs. (1)–(4) on the physical plane can be transformed into corresponding equations on the computation plane containing partial derivatives with respect to $\xi$ and $\eta$. While deriving the transformed equations we apply the forms of (9) and (10). In this way equations will be valid for quite general cases, not only for the special one specified by Eqs. (11).

The $x$ and $y$ components of the Navier–Stokes equations, (1) and (2), will be transformed as follows

$$\begin{aligned} &\frac{\partial u}{\partial \tau} + \left(u\frac{\partial y}{\partial \eta} - v\frac{\partial x}{\partial \eta}\right)\frac{\partial u}{\partial \xi}\frac{1}{J} + \left(v\frac{\partial x}{\partial \xi} - u\frac{\partial y}{\partial \xi}\right)\frac{\partial u}{\partial \eta}\frac{1}{J} \\ &\quad = -\left(\frac{\partial y}{\partial \eta}\frac{\partial p}{\partial \xi} - \frac{\partial y}{\partial \xi}\frac{\partial p}{\partial \eta}\right)\frac{1}{J} + \frac{1}{Re}\left(\alpha\frac{\partial^2 u}{\partial \xi^2} + \gamma\frac{\partial^2 u}{\partial \eta^2} + \varphi\frac{\partial u}{\partial \xi} + \sigma\frac{\partial u}{\partial \eta}\right)\frac{1}{J^2} - a_{0x}\,; \end{aligned} \tag{14}$$

$$\frac{\partial v}{\partial \tau} + \left(u\frac{\partial y}{\partial \eta} - v\frac{\partial x}{\partial \eta}\right)\frac{\partial v}{\partial \xi}\frac{1}{J} + \left(v\frac{\partial x}{\partial \xi} - u\frac{\partial y}{\partial \xi}\right)\frac{\partial v}{\partial \eta}\frac{1}{J}$$
$$= -\left(\frac{\partial x}{\partial \xi}\frac{\partial p}{\partial \eta} - \frac{\partial x}{\partial \eta}\frac{\partial p}{\partial \xi}\right)\frac{1}{J} + \frac{1}{Re}\left(\alpha\frac{\partial^2 v}{\partial \xi^2} + \gamma\frac{\partial^2 v}{\partial \eta^2} + \varphi\frac{\partial v}{\partial \xi} + \sigma\frac{\partial v}{\partial \eta}\right)\frac{1}{J^2} - a_{0y}\,. \tag{15}$$

The dilation $\Theta$ (3) transforms as

$$\Theta = \left(\frac{\partial y}{\partial \eta}\frac{\partial u}{\partial \xi} - \frac{\partial y}{\partial \xi}\frac{\partial u}{\partial \eta} + \frac{\partial x}{\partial \xi}\frac{\partial v}{\partial \eta} - \frac{\partial x}{\partial \eta}\frac{\partial v}{\partial \xi}\right)\frac{1}{J}\,. \tag{16}$$

The Poisson equation for pressure (4) will have the form

$$\alpha\frac{\partial^2 p}{\partial \xi^2} + \gamma\frac{\partial^2 p}{\partial \eta^2} + \varphi\frac{\partial p}{\partial \xi} + \sigma\frac{\partial p}{\partial \eta} = 2J\left(\frac{\partial u}{\partial \xi}\frac{\partial v}{\partial \eta} - \frac{\partial u}{\partial \eta}\frac{\partial v}{\partial \xi}\right) - J^2\frac{\partial \Theta}{\partial \tau}\,. \tag{17}$$

Boundary conditions for pressure, expressions (6) and (8) will be transformed as

$$R = R_1 : \frac{\partial p}{\partial \eta} = \frac{1}{ReJ^2}\left[\frac{\partial x}{\partial \eta}\left(\gamma\frac{\partial^2 u}{\partial \eta^2} + \sigma\frac{\partial u}{\partial \eta}\right) + \frac{\partial y}{\partial \eta}\left(\gamma\frac{\partial^2 v}{\partial \eta^2} + \sigma\frac{\partial v}{\partial \eta}\right)\right] - \frac{\partial x}{\partial \eta}a_{0x} - \frac{\partial y}{\partial \eta}a_{0y}\,; \tag{18}$$

$$R = R_2 : \frac{\partial p}{\partial \eta} \cong \left(\frac{\partial p}{\partial \eta}\right)_{\text{pot}}\,. \tag{19}$$

In Eqs. (14)–(18) variables $\alpha, \gamma, \varphi$ and $\sigma$ are defined as follows

$$\alpha = g_{22} = \left(\frac{\partial x}{\partial \eta}\right)^2 + \left(\frac{\partial y}{\partial \eta}\right)^2; \qquad \gamma = g_{11} = \left(\frac{\partial x}{\partial \xi}\right)^2 + \left(\frac{\partial y}{\partial \xi}\right)^2;$$

$$\varphi = \frac{1}{J}\left[\frac{\partial x}{\partial \eta}\left(\alpha\frac{\partial^2 y}{\partial \xi^2} + \gamma\frac{\partial^2 y}{\partial \eta^2}\right) - \frac{\partial y}{\partial \eta}\left(\alpha\frac{\partial^2 x}{\partial \xi^2} + \gamma\frac{\partial^2 x}{\partial \eta^2}\right)\right]; \tag{20}$$

$$\sigma = \frac{1}{J}\left[\frac{\partial y}{\partial \xi}\left(\alpha\frac{\partial^2 x}{\partial \xi^2} + \gamma\frac{\partial^2 x}{\partial \eta^2}\right) - \frac{\partial x}{\partial \xi}\left(\alpha\frac{\partial^2 y}{\partial \xi^2} + \gamma\frac{\partial^2 y}{\partial \eta^2}\right)\right]. \tag{21}$$

In these equations $J$ is the Jacobian defined by Eq. (12), $g_{11}$ and $g_{22}$ are elements of the metric tensor. Because of the structure of transformation (9) and (10) the grid is always orthogonal. Hence the off-diagonal elements of the metric tensor $g_{12} = g_{21} = 0$. That is also the reason why the mixed second derivatives are missing from the equations above, see [4].

Since the mapping is given by elementary functions, all of the metric parameters and coordinate derivatives can be computed from closed forms. In this way the numerical differentiation of coordinates subjected to numerical errors can be avoided.

It can be shown by using Eqs. (9), (10), (12) and (20) that when $g(\xi)$ is a linear function, as in Eq. (11), then $\varphi = 0$. If $f$ is a linear function of $\eta$, e.g., when $a_1 = 0$ in Eq. (11), then $\sigma = 0$, too, as can be shown using Eqs. (9), (10), (12) and (21). In these cases our equations can be simplified further, and the grid aspect ratio will become constant. By choosing the number of grid points in directions $\xi$ and $\eta$ properly, this constant can be set to unity resulting in conformal transformation [4].

## 4. Numerical approach

A computational code was developed for the solution of the problem. The governing equations are solved by the finite difference method. The time derivatives in the Navier–Stokes equations (14) and (15) are approximated by forward differences. Fourth order central difference scheme is used for the diffusion terms and pressure derivatives except for the points in the vicinity of the boundary where the proper stencils are not available. In these points fourth order difference formulae were derived

based on inner points by using the Taylor series. The widely used modified third order upwind scheme proposed by Kawamura [9] proved to be successful in handling the convective terms in the Navier–Stokes equations.

The equations of motion are integrated explicitly giving the velocity distribution at every time step. Since the computational grid is fixed on both the computational and physical planes, there is no need for interpolation for initial conditions at all. In the knowledge of the velocity distribution in an arbitrary time step, the pressure is calculated from Eq. (17) by using the successive over-relaxation method (SOR). Since the dilation $\Theta^{n+1}$ is chosen to be zero at every time step [13], the time derivative of $\Theta$ in this equation is approximated as

$$\frac{\partial \Theta^n}{\partial \tau} = \frac{\partial \Theta^n}{\partial t} \simeq \frac{\Theta^{n+1} - \Theta^n}{\Delta t} = -\frac{\Theta^n}{\Delta t} . \tag{22}$$

where superscripts $n$ and $n+1$ refer to the $n$th and the $(n+1)$th time step.

The pressure on the cylinder surface is calculated by the third order formula derived from the Taylor series at every time step

$$p_{i,1} = \frac{-p_{i,3} + 4p_{i,2} - 2\left.\frac{\partial p}{\partial \eta}\right|_{i,1}}{3} .$$

## 5. Results and discussion

The computational grid used is a 145×79 O-mesh, part of the grid points of which is shown in Fig. 2. The diameter of the outer boundary of computation is $30D$. For the sake of simplicity $\Delta\xi = \Delta\eta = 1$ was chosen on the computational plane. For all calculations $\Delta t = 0.001$ dimensionless time step was used.

Computations were carried out for the flow around a fixed circular cylinder for different Reynolds numbers. The results obtained are contained in Table 1. Here $Re$ is the Reynolds number, $S$ is the Strouhal number which is a dimensionless frequency of vortex shedding, $C_{D\text{mean}}$ is the time mean

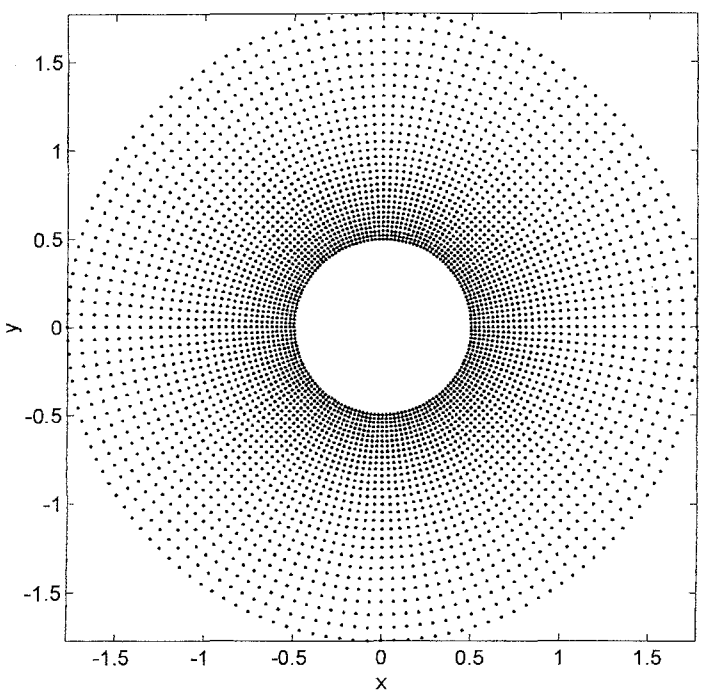


**Fig. 2.** Near grid points

**Table 1.**

| $Re$ | $S$ | $C_{D\text{mean}}$ |
|---|---|---|
| 10 | 0 | 2.905 |
| 20 | 0 | 2.087 |
| 40 | 0 | 1.552 |
| 60 | 0.137 | 1.407 |
| 80 | 0.151 | 1.357 |
| 100 | 0.167 | 1.332 |
| 120 | 0.176 | 1.317 |
| 140 | 0.179 | 1.311 |
| 160 | 0.186 | 1.311 |
| 180 | 0.189 | 1.310 |
| 200 | 0.195 | 1.311 |
| 220 | 0.196 | 1.318 |
| 400 | 0.220 | 1.355 |
| 600 | 0.228 | 1.378 |
| 800 | 0.236 | 1.392 |
| 1000 | 0.236 | 1.398 |

drag coefficient. Figure 3 shows a comparison between the calculated Strouhal numbers shown in Table 1 and the results of Roshko's [14] experiments. Measured (see [15]) and calculated mean drag coefficients (see Table 1) can be seen in Fig. 4.

Having a glance at Figs. 3 and 4, it can be stated that the agreement between experimental and calculated results is very good up to about $Re = 200$. It is proved in [6] that the flow around a circular cylinder becomes unstable at about $Re = 190$. This instability leads to three-dimensionality. $S$ and $C_D$ values are overestimated beyond this $Re$ number by using two-dimensional methods.

Figures 5–10 are related to computations for fixed cylinders for which Re=180. Figures 5 and 6 show the variation of lift coefficient $C_L$, skin friction lift coefficient $C_{Lf}$, drag coefficients $C_D$ and $C_{Df}$ with dimensionless time $t$, respectively. Having a glance at these figures we can see that only

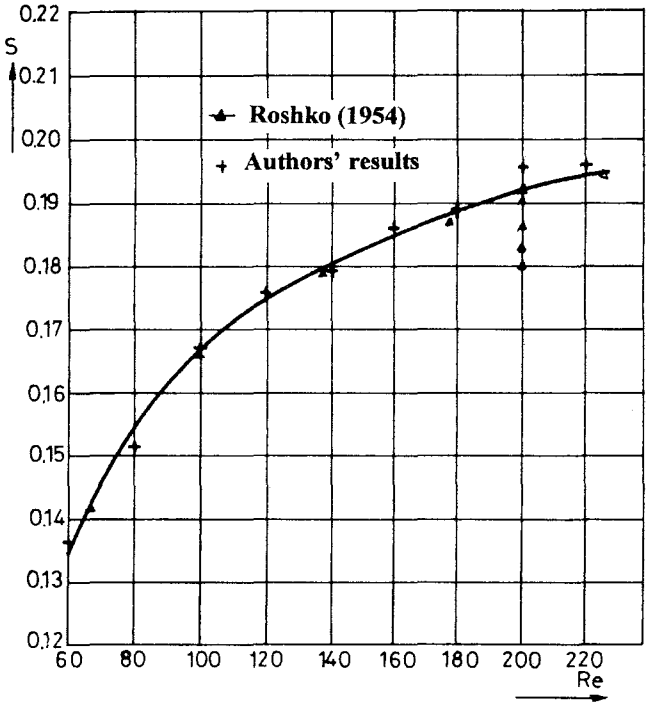


**Fig. 3.** Strouhal number *vs.* Reynolds number

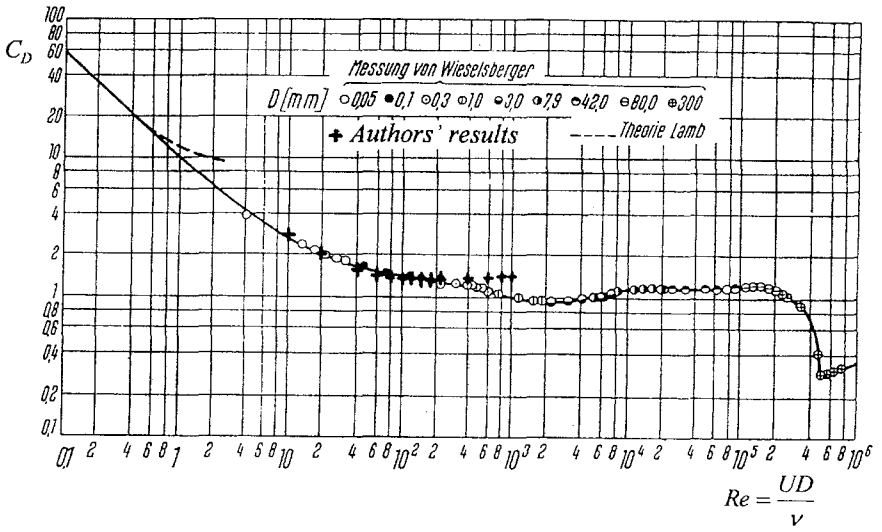


**Fig. 4.** Time mean drag coefficient *vs.* Reynolds number

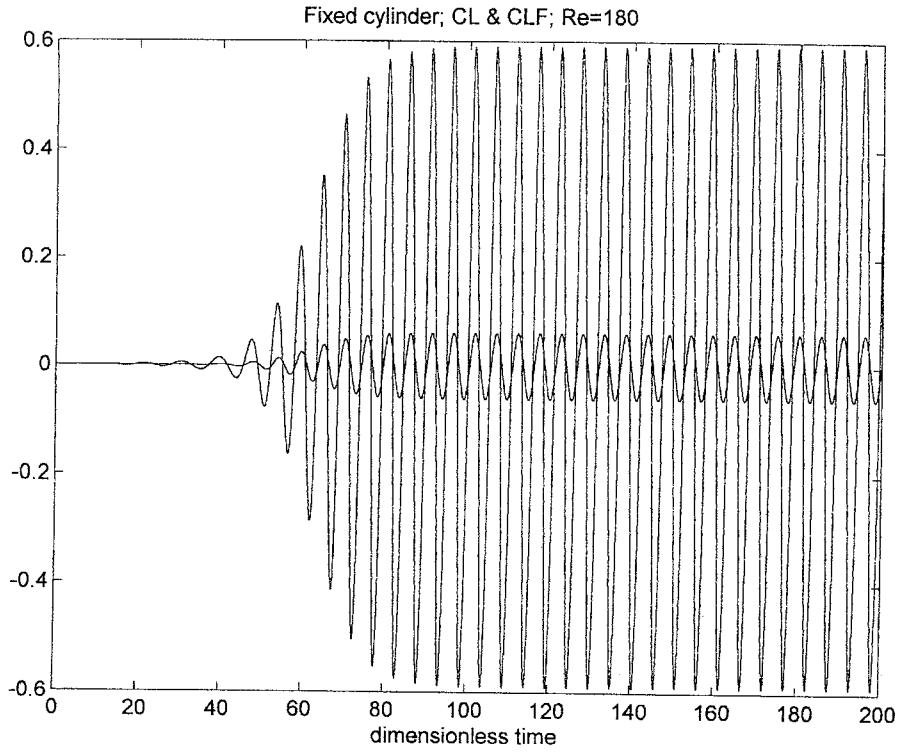


**Fig. 5.** Lift coefficients *vs.* time

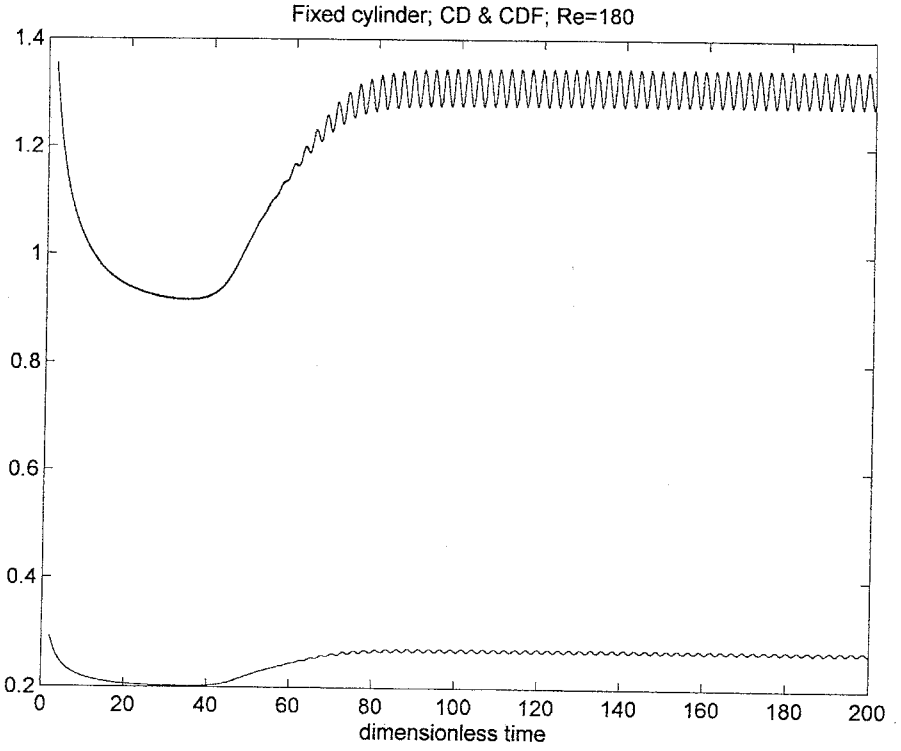


**Fig. 6.** Drag coefficients *vs.* time

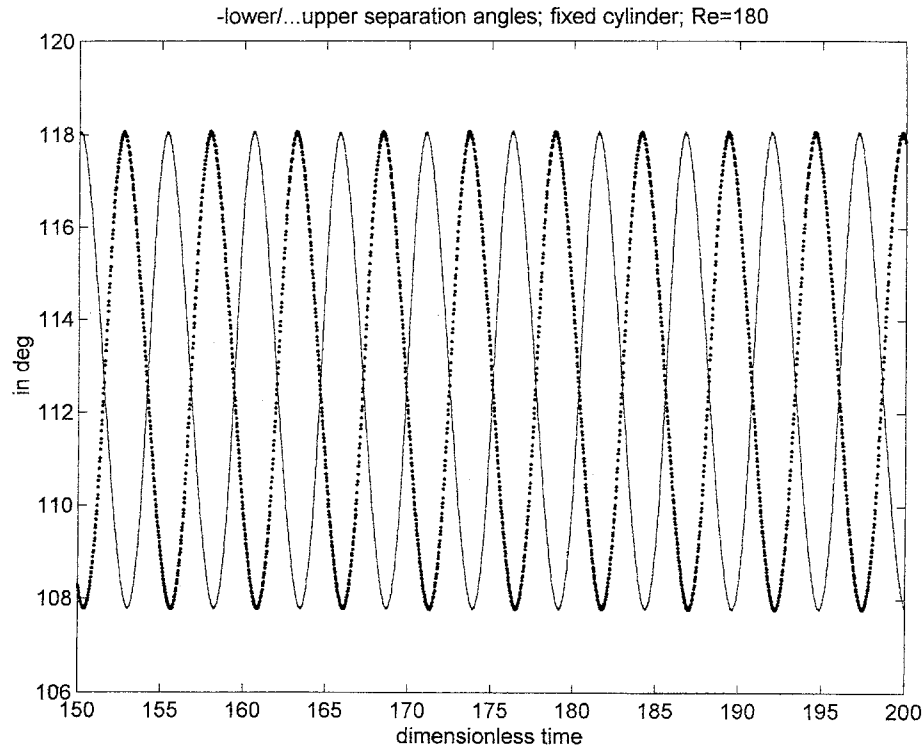


**Fig. 7.** Separation angles *vs.* time

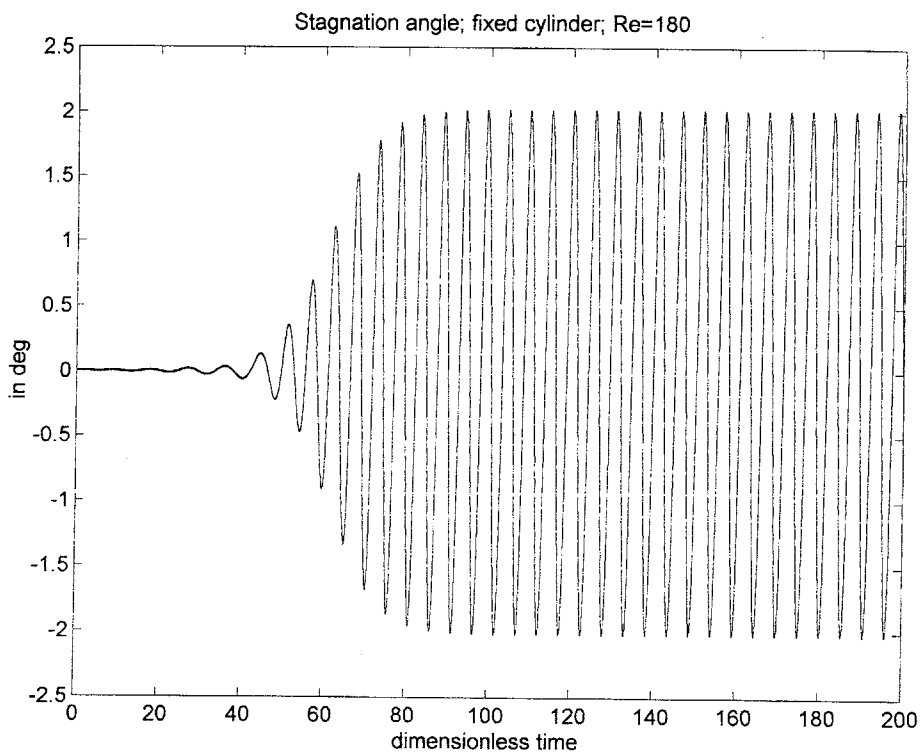


**Fig. 8.** Stagnation angle *vs.* time

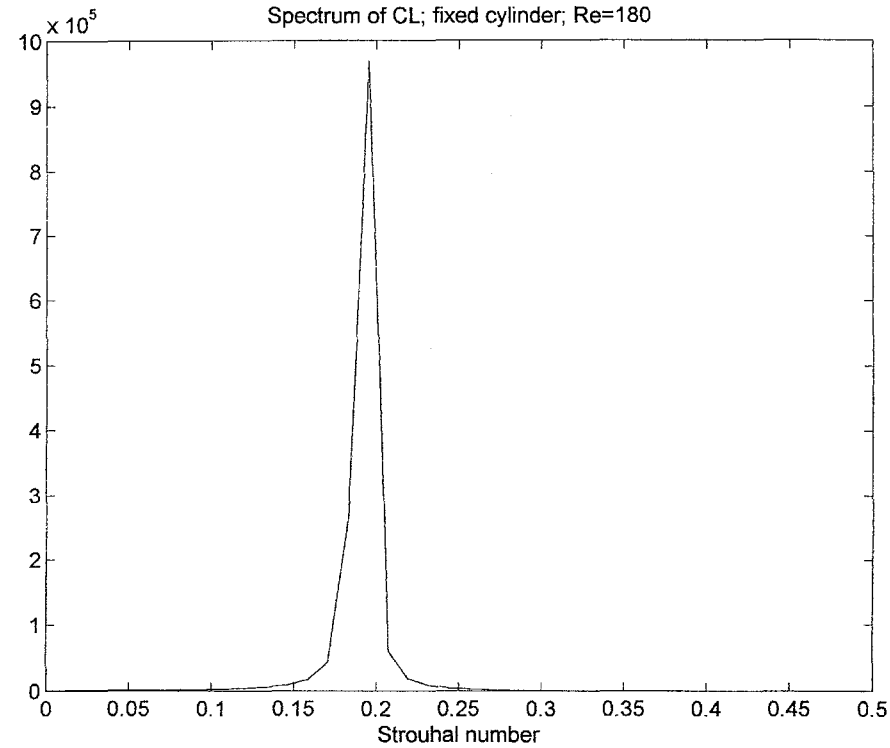


**Fig. 9.** Spectrum of lift coefficient

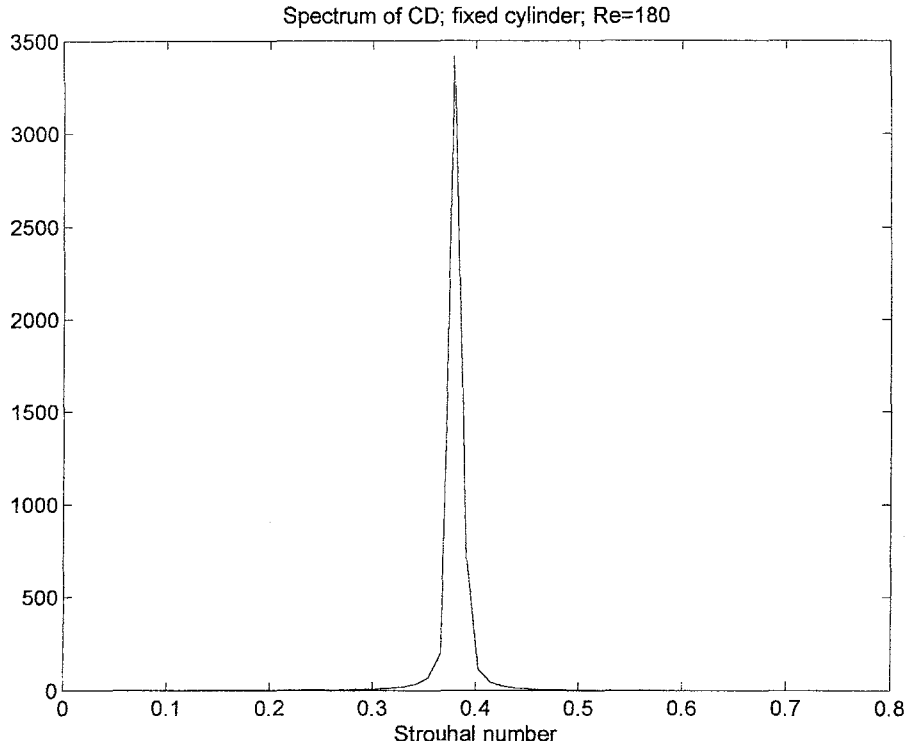


**Fig. 10.** Spectrum of drag coefficient

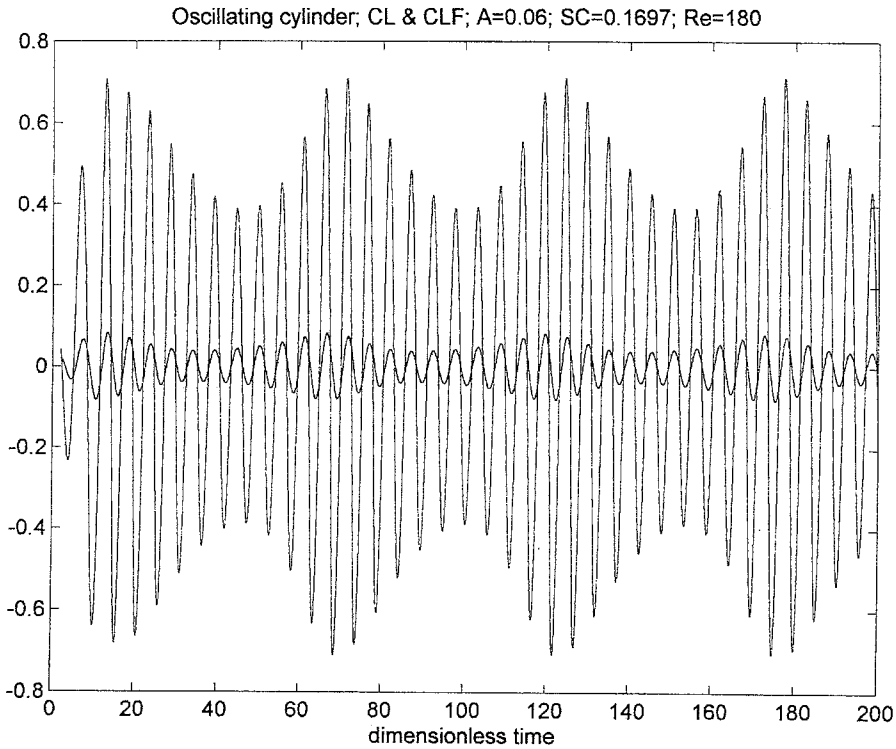


**Fig. 11.** Lift coefficient *vs.* time

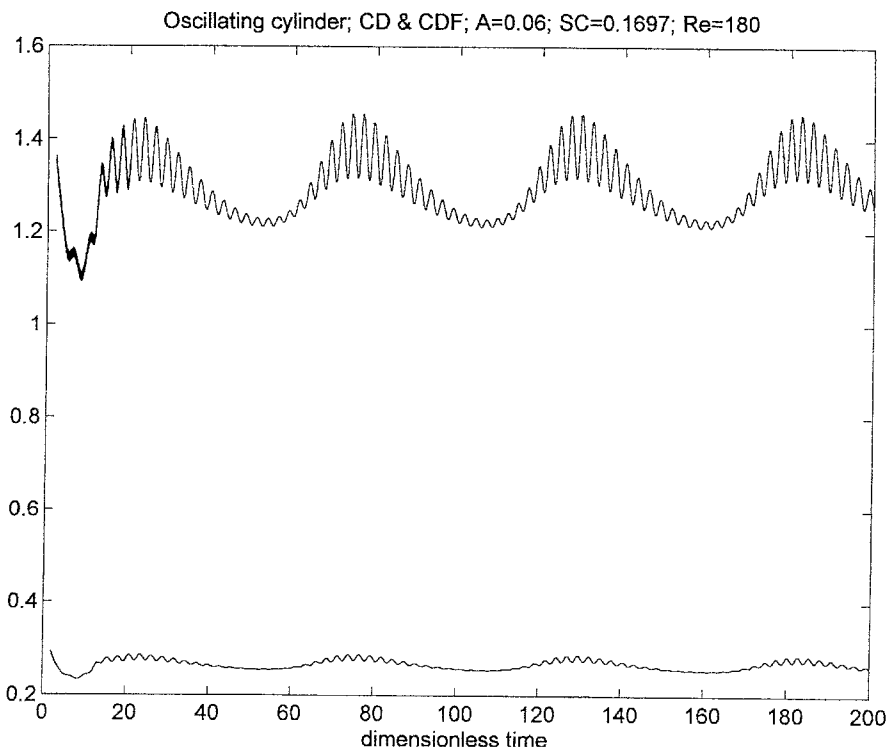


**Fig. 12.** Drag coefficient *vs.* time

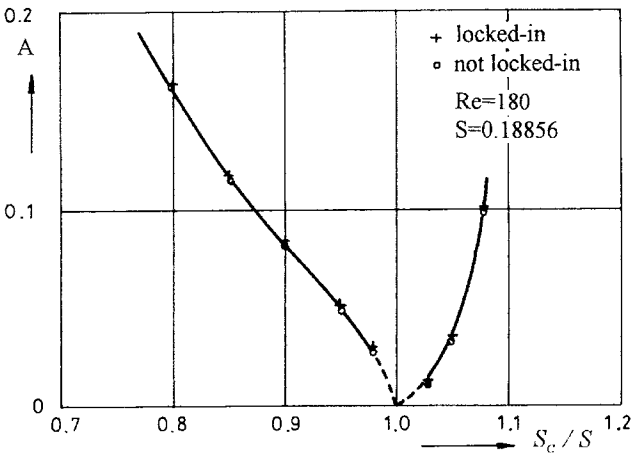


**Fig. 13.** Bounds for locked-in vortex shedding due to crossflow cylinder oscillation

small parts of the lift and drag coefficient are due to friction; larger parts are due to pressure. It can be seen that after some transitional period the vortex shedding becomes regular. As it is known the frequency of oscillation for the lift coefficient is equal to that of the vortex shedding, and the oscillation frequency for the drag coefficient is double of it.

Figure 7 shows the locations of the lower and upper separation points changing with time. These points are determined by using the condition of zero shear stress on the wall. These angles are measured from the point on the cylinder facing upstream. It can be seen that these angles are oscillating with the frequency of vortex shedding, and, as it is expected, there is approximately half wavelength shift between these two signals. A kind of stagnation point can be defined even in viscous flow where the velocity is zero on the wall. The stagnation angle corresponds to points of zero wall vorticity, $\omega_w = (\partial u/\partial y - \partial v/\partial x)$, [2]. The variation of stagnation angle can be seen in Fig. 8. The agreement between the present results and those of in [2] is good considering both separation and stagnation angles.

By applying the Fast Fourier Transform (FFT) for the regular parts of these oscillating signals their spectra can be obtained. Figures 9 and 10 show the spectra of the lift and drag coefficients, respectively. The frequency of vortex shedding can be determined from the location of the spectrum peaks. The value of Strouhal number belonging to the lift spectrum peak means the nondimensional frequency of vortex shedding. The location of the corresponding peak in the spectrum of drag gives double of the vortex shedding frequency.

Computations were also carried out for flows about cylinders which are vibrated mechanically either in crossflow or in-line directions. It is well known that if the amplitude of cylinder oscillation is large enough, the frequency of vortex shedding is synchronizing with that of the cylinder vibration. This phenomenon is called lock-in. In this case the oscillating signals and their spectra will become similar to the ones for fixed cylinders.

Results will be shown for cases where the amplitude of crossflow oscillation is smaller than the bound value for lock-in. Reynolds number is $Re = 180$, the dimensionless amplitude of oscillation $A = 0.06$, the dimensionless frequency of cylinder oscillation $S_C = 0.1697$. Figures 11 and 12 show the variation of lift coefficients $C_L$ and $C_{Lf}$, further drag coefficients $C_D$ and $C_{Df}$ with dimensionless time $t$. Having a glance at these figures we can see the frequency modulations.

The amplitude bounds of locked-in vortex shedding due to forced crossflow oscillation of a circular cylinder for $Re = 180$ were also investigated by the authors. Bounds for dimensionless amplitude $A$ are shown in Fig. 13 as a function of the dimensionless frequency of cylinder oscillation $S_C/S$. Here $S$ is the Strouhal number for $Re = 180$, $S_C$ is the Strouhal number based on the frequency of cylinder oscillation. Since this investigation requires the running of code many times the necessary CPU time is very long.

## 6. Concluding remarks

The finite difference method has been applied for the direct numerical simulation of unsteady, laminar incompressible fluid flow about fixed and oscillating circular cylinders placed in otherwise uniform flows. Primitive variable formulation has been chosen, and a separate equation is used for pressure $p$ [13]. Equations are derived in a non-inertial system fixed to the cylinder. By using boundary fitted coordinates, interpolation of the boundary conditions becomes unnecessary. The choice of a grid fixed to the moving cylinder assures that the grid has to be generated only once during the computation, and it also eliminates the need for interpolation of the initial values at every time step. An orthogonal transformation is used to map the physical plane to the computational one, and the grid density can be controlled. Since the transformation is given by elementary functions, coordinate derivatives and metric parameters can be obtained without using numerical differentiations, leading to more accurate solution. Time derivatives are approximated by forward differences, space derivatives by fourth order central differences except for the convective terms for which a third order modified scheme was used [9]. Velocity values are obtained by integrating the Navier–Stokes equations explicitly, and SOR method is used for the determination of the pressure distribution at every time step. By using the velocity and pressure distributions several other flow properties are derived. The vortex shedding frequency is obtained by applying the FFT for the computed oscillating signals.

Extensive computations have been carried out for fixed cylinders to test the computational results against experimental ones. The calculated time mean drag coefficients and dimensionless vortex shedding frequencies agrees well with the corresponding experimental values up to about $Re = 200$. Beyond this $Re$ number the present two-dimensional method overestimates the $C_D$ and $S$ values. This experience is in accord with that of authors [6], who showed that the flow around a fixed circular cylinder becomes unstable and three-dimensional at about $Re = 190$. Hence two-dimensional methods should not be used beyond this $Re$ value. Due to lack of space only small fraction of the computational results are included in the paper. The determination of separation and stagnation angles was based on the conditions of vanishing shear stress and vorticity on the cylinder wall, respectively. These values agree well with ones shown in [2].

Authors run the code for computation of flow about oscillating cylinders both in crossflow and inline directions, many times, too. The amplitude bounds of locked-in vortex shedding due to forced crossflow oscillation of a circular cylinder for $Re = 180$ are shown in Fig. 13. The determination of this kind of curves requires large amount of CPU time. So far the authors had no opportunity to compare this last result with those of experimental or other theoretical investigations.

The authors' plan for the future is to

1. introduce higher order time differencing schemes;
2. compare results for oscillating cylinders with test results;
3. investigate the effect of $Re$ number on the amplitude boundaries for lock-in;
4. investigate the effect of cylinder cross-sectional configuration on the flow;
5. extend the code to 3-D.

## Acknowledgements

The authors would like to thank Professor A. Nyíri of the University of Miskolc (UM) for useful discussions regarding this work. They would also like to acknowledge the activities of Mr. G. Kósa of UM, of Mr. K. Miyano of Nagaoka University of Technology (NUT), who helped us in the development of the computer code, and of Mr. M. Koide, also of NUT, for running the code for several test cases.

## REFERENCES


[1] P.W. Bearman. Developments in the understanding of bluff body flows. *Proceedings of the Int. Conf. on Fluid Engineering*, Vol. **1**, Tokyo, Japan, 53–61, 1997.

[2] M. Braza, P. Chassaing, H.H. Minh. Numerical study and physical analysis of the pressure and velocity fields in the near wake of a circular cylinder. *Journal of Fluid Mechanics*, **165**, 79–130, 1986.

[3] R. Chilukuri. Incompressible laminar flow past a transversely vibrating cylinder. *Journal of Fluids Engineering*, **109**, 166–171, 1987.

[4] C.A.J. Fletcher. *Computational Techniques for Fluid Dynamics*, Vol. 2. Springer, 2nd Ed., Berlin, 1997.

[5] F.H. Harlow, J.E. Welch. Numerical calculation of time-dependent viscous incompressible flow of fluid with free surface. *Physics of Fluids*, **8**, 2182–2189, 1965.

[6] R.D. Henderson, D. Barkley. Secondary instability in the wake of a circular cylinder. *Physics of Fluids*, **8**, 1683–1685, 1996.

[7] S.E. Hurlbut, M.L. Spaulding, F.M. White. Numerical solution for laminar two dimensional flow about a cylinder oscillating in a uniform stream. *Journal of Fluids Engineering*, **104**, 214–222, 1982.

[8] G.E. Karniadakis, G.S. Triantafyllou. Frequency selection and asymptotic states in laminar wakes. *Journal of Fluid Mechanics*, **199**, 441–469, 1989.

[9] T. Kawamura. Computation of high Reynolds number flow around a circular cylinder with surface roughness. *Proceedings of the 22nd Aerospace Sciences Meeting, Reno, Nevada*, AIAA-84-0340, 1–11, 1984.

[10] J. Kim, P. Moin. Application of a fractional-step method to incompressible Navier–Stokes equations. *Journal of Computational Physics*, **59**, 308–323, 1985.

[11] J.R. Meneghini, P.W. Bearman. Numerical simulation of high amplitude oscillatory flow about a circular cylinder. *Journal of Fluids and Structures*, **9**, 435–455, 1995.

[12] K. Ogane, H. Sakuta, H.M. Bea, T. Takahashi, M. Shirakashi. Numerical analysis for lock-in phenomenon of vibrating cylinder in uniform flow. *Proceedings of the 7th Int. Conf. on Numerical Methods in Laminar and Turbulent Flow*, Vol. **2**, Stanford, U.S.A., 1374–1384, 1991.

[13] P.J. Roache. *Computational Fluid Dynamics*. Hermosa Publishers, Albuquerque, 1982.

[14] A. Roshko. On the development of turbulent wakes from vortex streets. *NACA Rep.*, 1191, 1954.

[15] H. Schlichting. *Grenzschicht-Theorie*. Verlag G. Braun, Karlsruhe, 1965.